

Metallophobic Coatings to Enable Shape Reconfigurable Liquid Metal Inside 3D Printed Plastics

Jinwoo Ma, Vivek T. Bharambe, Karl A. Persson, Adam L. Bachmann, Ishan D. Joshipura, Jongbeom Kim, Kyu Hwan Oh, Jason F. Patrick, Jacob J. Adams, and Michael D. Dickey*



Cite This: *ACS Appl. Mater. Interfaces* 2021, 13, 12709–12718



Read Online

ACCESS |



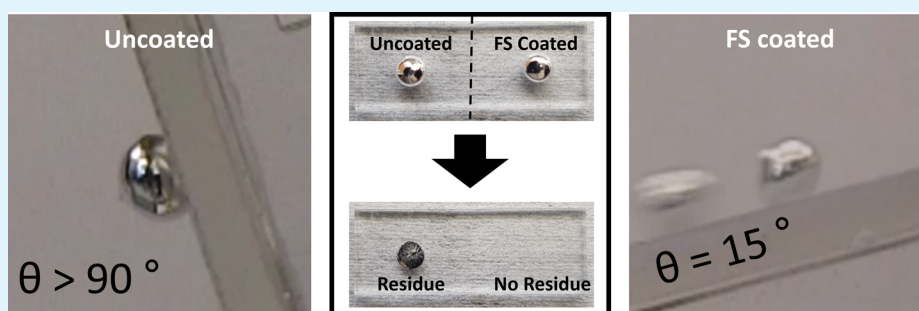
Metrics & More



Article Recommendations



Supporting Information



ABSTRACT: Liquid metals adhere to most surfaces despite their high surface tension due to the presence of a native gallium oxide layer. The ability to change the shape of functional fluids within a three-dimensional (3D) printed part with respect to time is a type of four-dimensional printing, yet surface adhesion limits the ability to pump liquid metals in and out of cavities and channels without leaving residue. Rough surfaces prevent adhesion, but most methods to roughen surfaces are difficult or impossible to apply on the interior of parts. Here, we show that silica particles suspended in an appropriate solvent can be injected inside cavities to coat the walls. This technique creates a transparent, nanoscopically rough (10–100 nm scale) coating that prevents adhesion of liquid metals on various 3D printed plastics and commercial polymers. Liquid metals roll and even bounce off treated surfaces (the latter occurs even when dropped from heights as high as 70 cm). Moreover, the coating can be removed locally by laser ablation to create selective wetting regions for metal patterning on the exterior of plastics. To demonstrate the utility of the coating, liquid metals were dynamically actuated inside a 3D printed channel or chamber without pinning the oxide, thereby demonstrating electrical circuits that can be reconfigured repeatedly.

KEYWORDS: liquid metal, additive manufacturing, reconfigurable circuit, metallophobic surface, liquid metal actuation, 4D printing

INTRODUCTION

The combination of fluidity and the metallic conductivity of liquid metals is promising^{1–3} for stretchable electronics,^{4–8} soft composites,^{9–14} and catalysts.^{15–17} In particular, gallium-based liquid metals such as eutectic gallium indium (EGaIn, the alloy used here) are compelling, because they have melting points below room temperature yet do not have the toxicity issues of mercury. Patterning liquid metals is important for forming useful shapes such as stretchable antennas, electrodes, wiring, optical structures, and interconnects.^{18–21}

In addition to being soft, one of the most exciting aspects of liquid metals is the ability to pattern them in ways that simply are not possible with solid metals. For example, liquids can be direct-write printed, wetted to surfaces, or injected into cavities and microfluidic channels. Injection is particularly attractive for adding a metallic function to a three-dimensional (3D) printed polymer. That is, a plastic part printed with cavities can then be backfilled with metal.^{22–27} A number of approaches exist for metallizing 3D printed parts (i.e., spraying, electroless plating,

sputtering),^{28–32} but none are as simple as injecting metal. This approach takes advantage of the three-dimensional complexity made possible by additive manufacturing (AM) to create, for example, embedded helical filaments, radio frequency antenna arrays, and high-frequency coaxial transmission lines.

Interfacial effects dominate the behavior of the metal in sub-millimeter cavities.³³ Injecting the metal into the part requires applying sufficient pressure to overcome interfacial forces. Yet, once the metal is within a part, it is typically difficult to remove it completely due to the adhesion with the surface. Because it is a liquid, it is possible to change the shape of the metal in an

Special Issue: Novel Stimuli-Responsive Materials for 3D Printing

Received: September 30, 2020

Accepted: November 17, 2020

Published: November 25, 2020



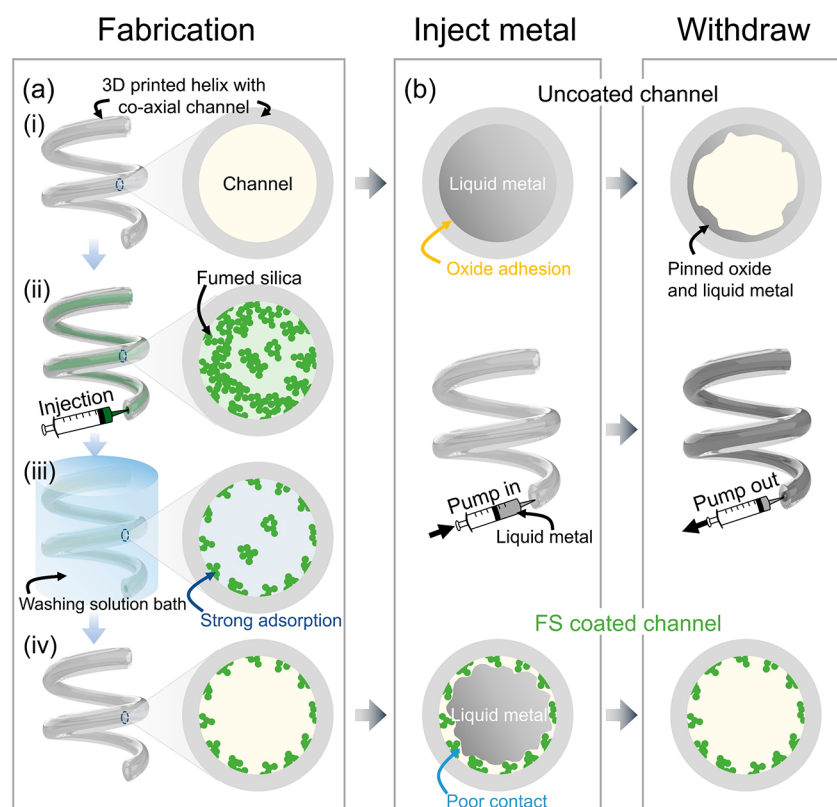


Figure 1. Fabrication and operation of metallophobic 3D printed plastic (depicted here as a 3D printed hollow helix). (a) FS particles deposit on plastic surfaces by either the immersion of the plastic in the FS solution or the injection of the FS solution into a channel for 2 min. The weakly bound FS clusters wash away, leaving behind a thin transparent coating. (b) The liquid metal adheres to untreated plastic, leaving behind residue when it is withdrawn. In contrast, the liquid metal can be pumped in/out of the FS-coated channel without leaving any liquid metal residue in the channel. The size of the FS clusters and the roughness at the interface of the liquid metal and coated FS are exaggerated to visualize them clearly.

otherwise static structure by pumping the metal in/out of cavities built into the 3D printed part; this is an unconventional approach to four-dimensional (4D) printing, in which functional fluids inside a 3D printed part change shape, which is the theme of this special issue. This paper focuses on a simple way to prevent adhesion so that the metal can easily move in and out of 3D printed structures by pumping. The ability to do so enables the possibility of reconfigurable metallic structures, such as shape-reconfigurable antennas and electromagnetic devices.³⁴

Liquid metals adhere to surfaces due to the presence of a thin native oxide layer that forms on the metal. To prevent the oxide from sticking to surfaces, several approaches have been explored, such as lowering the oxygen level,³⁵ using a strong acid or base to remove the oxide layer,^{36,37} introducing a slip layer between oxide and surface,³⁸ treating the surface of the liquid metal with particles,^{39–42} and making the surface “metallophobic” (the term metallophobic is used loosely here to refer to liquid metals with surface oxides).^{43–51} The oxide forms even at very low levels of oxygen; thus, sufficiently lowering the oxygen concentration is challenging. A strong acid or base is generally corrosive and provokes electrolysis under a small voltage less than 2 V, and therefore it is not desirable. Introducing a slip layer (that is, a thin liquid layer between liquid metal and the surface) requires the inclusion of a secondary cofluid, leaving very few attractive options.

Here, we sought to create a surface to which liquid metal does not adhere. Many groups have successfully developed metallophobic surfaces by making the surface nanoscopically

rough to place the metal in the Cassie–Baxter wetting state. The oxide-coated metal does not penetrate into the pores of the rough surface and therefore makes poor contact (and thus, poor adhesion). To make surfaces rough, researchers have used spray coatings,^{49,51} molding,⁴³ etching,⁴⁸ and sputtering.^{44,46,52} Although these approaches are appealing due to their simplicity, each of these methods only works on exposed (exterior) surfaces. For microfluidic applications, it is desirable to coat the interior walls of a channel, which is nontrivial. With some effort, it is possible to coat the walls of open-faced channels and then seal them with another planar surface, but such approaches are tedious and limited to simple, planar geometries.⁴⁹ Thus, existing approaches to create metallophobic surfaces are not easy to apply to the interior of cavities, such as those found on the interior of complex 3D printed objects. In addition, existing methods, such as commercial Neverwet, create optically hazy coatings;⁴⁹ in contrast, the coatings here are transparent.

In this study, we present a simple method to coat the interior and exterior of plastics and 3D printed parts to make them rough and thereby prevent the adhesion of liquid metal. We coated various plastics by immersing 3D printed parts or slabs of common thermoplastics in a solution of fumed silica (FS) suspended in solvent (e.g., chloroform). A solution-based coating is appealing, because the solution can be injected into the interior of parts and is therefore applicable to any fluid-accessible surface, such as fluidic channels. The coating solution causes the exposed surface of the resins to temporarily swell and/or plasticize and thereby promotes good adhesion

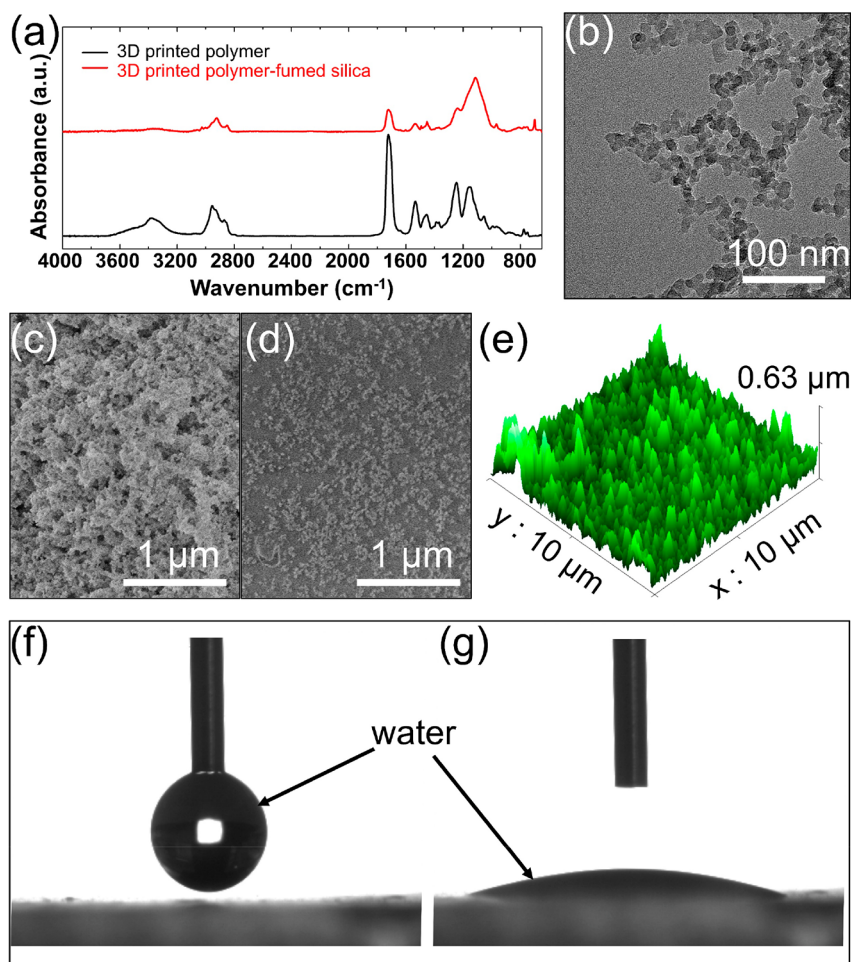


Figure 2. Characterization of the surface of 3D printed plastic that is metallophobic. (a) FT-IR ATR spectra of the plastic (black) and the FS-coated plastic (red). (b) A representative TEM image of the FS. SEM images of the FS-coated surface (c) before and (d) after a wash. (e) AFM of the FS-coated surface. (f, g) Optical images of a water droplet on the surface. The water droplet spread on the FS surface, showing that the coating is hydrophilic (yet, metallophobic).

between the particles and the surface. After the solution has been removed and the surface has been rinsed, particles remain adhered to the polymer. The resulting rough surface prevents metal adhesion on hydrophobic and hydrophilic surfaces, confirming that the roughness is responsible for making the surface nonwetting, rather than the surface chemistry. The transparent coating works well on common 3D printed polymers as well as other common plastics such as acrylic and polystyrene (the material used in disposable Petri dishes). Harnessing this metallophobic surface treatment, we demonstrate a reconfigurable circuit and a variable area capacitor by pumping liquid metal in and out of 3D printed cavities without any residue left behind.

■ RESULT AND DISCUSSION

We coated 3D printed plastics with the FS, which has a high specific surface area ($\sim 150 \text{ m}^2/\text{g}$), to introduce nanoscale roughness to the surface of a 3D printed plastic, as shown in Figure 1. We began our studies with a common commercial resin (RS-F2-GPCL-04, Formlabs) composed of methacrylic monomer, methacrylic oligomer, and a photo initiator. After printing polymeric structures, we rinsed the parts gently in an isopropyl alcohol (IPA) solution for 10 min to remove any residue that may have remained on the surface from printing.

The 3D print was then coated with the FS by either immersing the print in the FS/chloroform solution (1% w/v) for 2 min in a sonicator bath, which kept the FS well-distributed and eliminated large agglomerates ($>1 \mu\text{m}$), or injecting the solution into the channel. After 2 min, the device was washed using isopropyl alcohol and deionized (DI) water. The surface of the plastic slightly swells when immersed in the solvent (Figure S1), which facilitates contact between the FS and surface. On thermoplastics, the FS physically adsorbs to the surface by temporarily plasticizing and partially solubilizing the surface of the polymer with solvent. The plasticization makes the surface tacky and the chains at the surface mobilize, thereby promoting adhesion between the FS and the polymer surface. Solvents, such as water, do not produce a robust coating, since they do not swell the surface (coatings formed using water as a solvent did not prevent adhesion of the liquid metal when pumping the metal through coated channels). After the FS was coated on the polymer, the polymer showed a metallophobic nature. Thus, liquid metal can be actuated in the channel without any pinning of the oxide-coated metal (Figure 1b).

The deposited FS prevents adhesion of the liquid metal by forming a Cassie–Baxter-like state, as shown conceptually in Figure S2. To verify the FS was deposited on the surface, we utilized Fourier transform infrared spectroscopy in attenuated

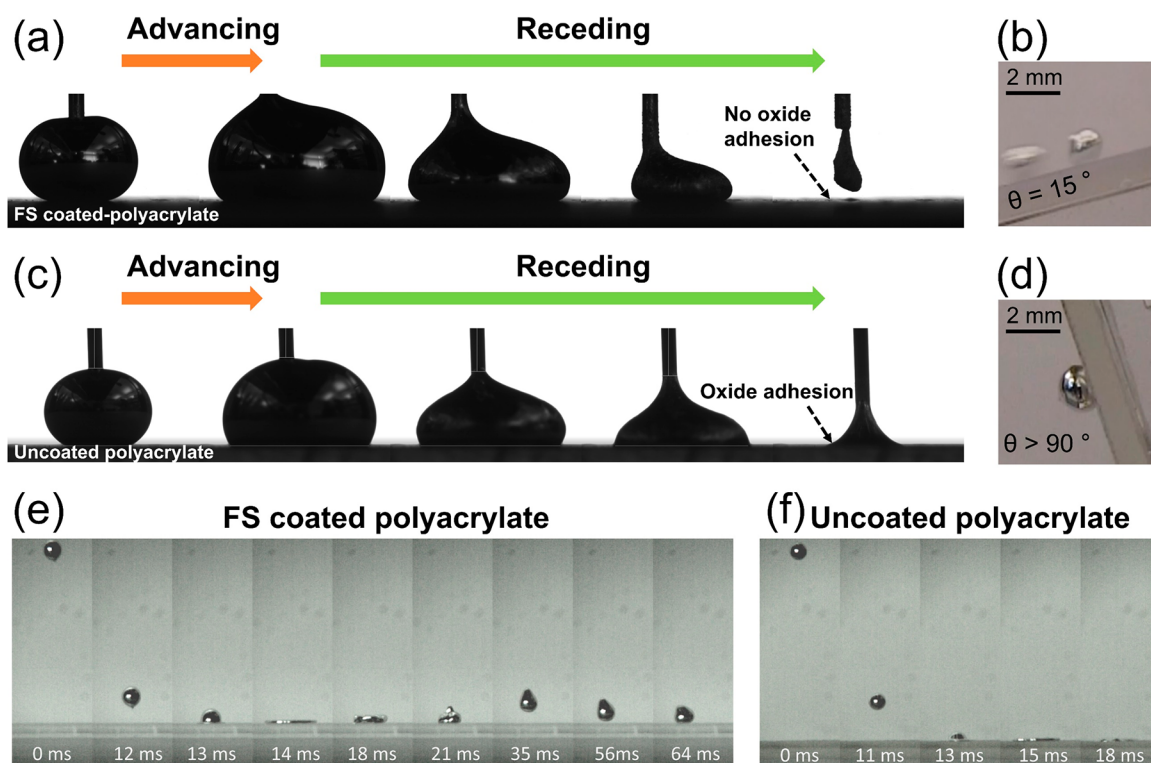


Figure 3. Comparison of pinning behaviors between the FS-coated (rough) surface and the uncoated (smooth) surface. (a) While EGaIn droplets receded from the FS-coated surface without pinning, (c) it pinned to the uncoated surface. (b) EGaIn droplet ($5 \mu\text{L}$) rolled off at 15° on the FS-coated surface, and (d) pinned on the uncoated surface. Sequential images of an EGaIn droplet ($5 \mu\text{L}$) falling from 15 cm onto an (e) FS-coated and (f) uncoated surface.

total reflection mode (FTIR-ATR). As shown in Figure 2a, the spectrum of the FS-coated surface (red) clearly indicates strong Si–O stretching at 1100 cm^{-1} , which is one of the representative peaks of the FS.⁵² Instead, the spectrum of the bare polymer surface showed the typical methacrylate peaks at 1720 and 1240 cm^{-1} , which is likely attributed to C=O stretching and C–O stretching, respectively.

The FS has not only a high specific surface area but nanoscale roughness, as shown in previous studies.^{53,54} We used transmission electron microscopy (TEM) to image the particles in the coating solution, as shown in Figure 2b. Although the particles form small clusters ($\sim 100 \text{ nm}$ clusters), image analysis of the microscopy image using ImageJ determined the average diameter of an individual silica particle to be $12.02 \pm 2.3 \text{ nm}$. After a coating (Figure 2c), a layer of particles remains on the surface, although many of these particles are removed by a rinse. The particles that remain are strongly adsorbed, as shown in Figure 2d. Clusters of the FS were deposited on the surface, forming island structures. The clusters have diameters close to 100 nm or less, thereby forming a nanoscale hierarchical structure, as the clusters are composed of the smaller particles ($\sim 12 \text{ nm}$, according to TEM images). The resulting nanostructured surface was further investigated with atomic force microscopy (AFM) to measure the roughness (Figure 2e, Figure S3). AFM revealed the peak-to-peak height of the FS clusters is generally less than 200 nm and the distance between the clusters is $\sim 300 \text{ nm}$. AFM also confirmed that the coated surface has a nanoscale roughness. As the FS is hydrophilic, the surface was also highly hydrophilic as shown in Figure 2f,g. The surface was sufficiently wet by water that the contact angle could not be measured; that is, the image in Figure 2g is a snapshot as the

water continued to spread. We include it just to prove the surface is hydrophilic despite being rough.

After coating the plastics with FS, we tested whether EGaIn adheres to the surface. To test for adhesion, we advanced a droplet (i.e., increasing the volume) against a surface and then subsequently receded it (i.e., decreasing the volume). The droplets recede and do not pin on treated surfaces (Figure 3a). In contrast, the metal pinned and adhered to the uncoated surfaces, leaving behind residue (Figure 3c).

We also measured the roll-off angle, which is an indicator of adhesion forces. The EGaIn droplet ($\sim 5 \mu\text{L}$) was put on the FS-coated substrate, and then the substrate was rotated slowly ($\sim 0.125 \text{ rpm}$). The photograph in Figure 3b is slightly blurry, because the droplet is moving. The EGaIn droplet rolled off from the coated surface at $14.8 \pm 2.1^\circ$ (Figure 3b, Video S1). We repeated the experiment on a noncoated substrate. Figure 3d shows that the droplet did not roll off from the uncoated substrate (Video S2), even if the substrate was rotated over 90° . The gallium oxide on the surface of the liquid metal adheres to the smooth substrate. This adhesion, combined with the mechanical strength of the oxide (surface yield stress of $\sim 0.3\text{--}0.5 \text{ N/m}$), keeps it from moving when tilted. Compared to Figure 3b, the image in Figure 3d is less blurry, since the droplet is not sliding down the tilted surface. With larger droplets (those with diameters larger than the capillary length, $\sim 2\text{--}3 \text{ mm}$), gravitational forces were sufficient to cause the upper portion of the EGaIn droplet to travel down the uncoated surface, even though the base of the drop remained pinned.

Prior studies have shown that surface roughness is critical for preventing adhesion, rather than the specific chemistry (and hydrophilicity/phobicity) of the surface.^{45,49} Thus, we

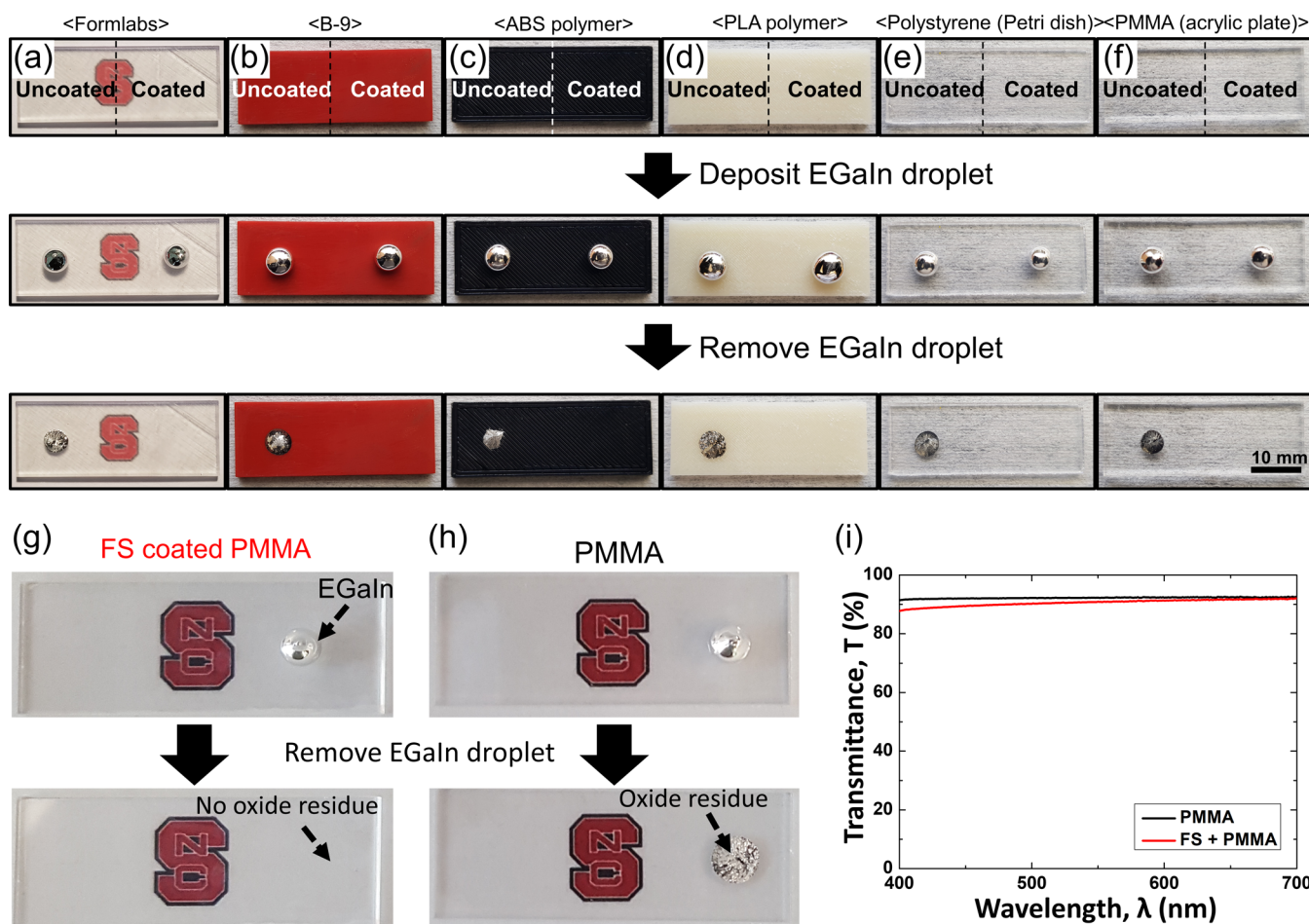


Figure 4. Common plastics can be coated with FS, thereby forming metallophobic surfaces that are not detectable by eye. The plastics include 3D printed polymers (a–d) and commercial polymers (e, f). The right-hand side of the substrates was coated with the FS and showed a metallophobic nature relative to the uncoated, left-hand side. (g, h) FS-coated PMMA shows a similar optical transparency to that of PMMA. (i) UV–Vis spectra of the FS-coated PMMA (red) and PMMA (black) in the visible range.

functionalized the FS-coated surface to be super-hydrophobic with trichloro(1*H*,1*H*,2*H*,2*H*-perfluorooctyl) silane to verify that it did not change the outcome. A surface exhibiting a super-hydrophobic nature (i.e., the contact angle of water was over 150°) also prevents liquid metal from pinning to the surface (Figure S4).

We further confirmed the metallophobicity by dropping liquid metal onto the surface and imaging with a high-speed camera (Figure 3e, Figure S5 for experimental setup, Video S3). These images show that a droplet (5 μ L) of liquid metal bounces off the surface when dropped from 15 cm. Note that the metal also bounced from the surface when dropped from up to \sim 70 cm. Above 75 cm the metal breaks into smaller droplets rather than bouncing. When dropped from 15 cm, the liquid metal adhered to the uncoated surface (Figure 3f, Video S4), since the oxide layer forms rapidly (microseconds, orders of magnitude faster than the milliseconds of this experiment),⁵⁵ which promotes adhesion to the substrate. Note that another approach for preventing adhesion in these types of experiments is to first coat the liquid metal with particles (rather than coating the particles on the substrate). Such structures are called “liquid marbles”. In such experiments, the marble adhered to a surface or splashed when dropped above a critical height,⁴⁰ presumably because the coating on the marble breaks as it splatters on the substrate. In contrast, the EGaln

droplets here bounced when dropped from a much higher height (70 cm vs 1–2 cm in the case of marbles), in a manner similar to water on super-hydrophobic surfaces. Thus, the initial height is substantially higher than the critical height of other liquid metal marble droplets.

We sought to evaluate the coating on various 3D printed plastic parts to demonstrate its versatility. We used a stereolithographic 3D printer (Form 2, Formlabs) to achieve fine feature sizes utilized for the tests. We used the clear resin of Form 2 (RS-F2-GPCL-04, Formlabs) as shown in Figure 4a. The print is sufficiently transparent to see through the substrate, which aids in visualization (the coating layer is optically undetectable by eye). In addition, to demonstrate that the method is widely applicable to common polymers, we coated polystyrene (PS), poly(methyl methacrylate) (PMMA), acrylonitrile butadiene styrene (ABS), poly(lactic acid) (PLA)-based polymer (fused deposition modeling based plastics), and other poly(methacrylic)-based polymer (digital light-processing-based plastics, B9Creation). We empirically varied the solvent composition to ensure that the treatments work as shown in Figure 4 (for the solvent information, please see Table S1). As a control, we only applied the FS coating to the right half (Figure 4a–f) by immersing the plastics partially. To test for metallophobicity, we advanced and receded a droplet of EGaln against each part. While receding the droplet, the

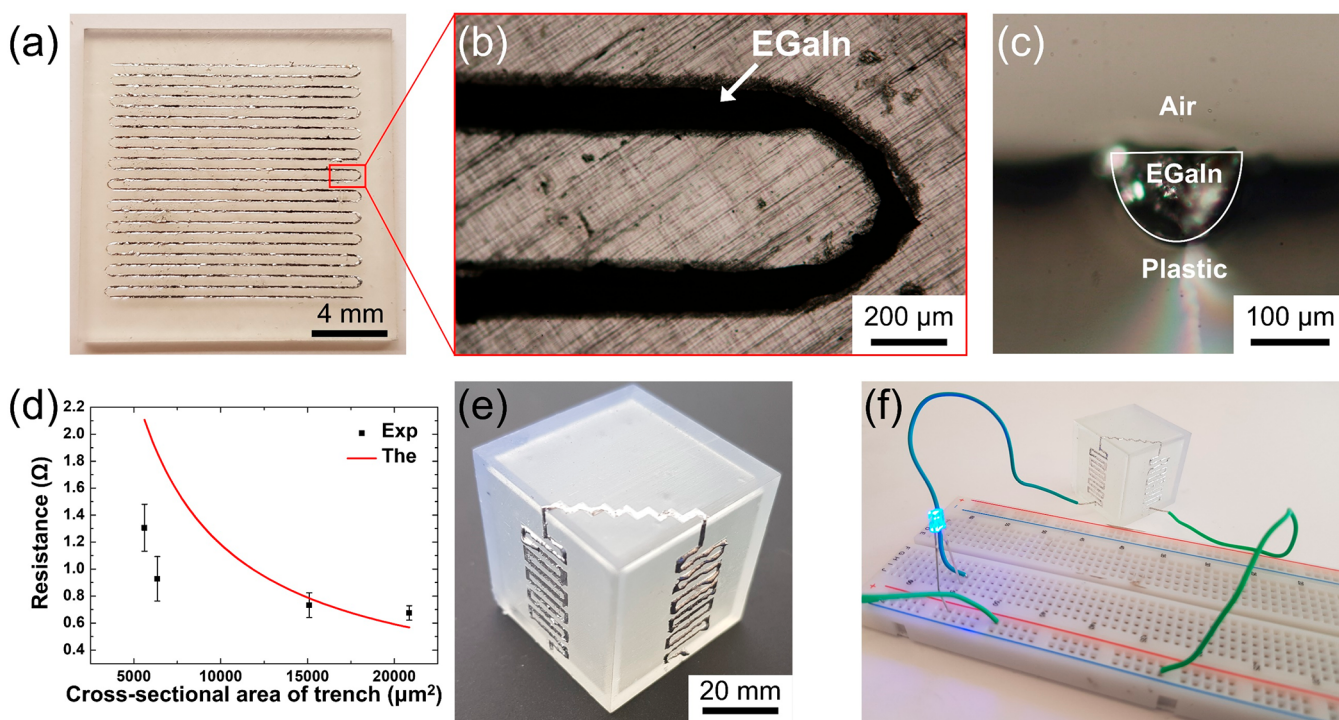


Figure 5. Selectively patterned liquid metal on the laser-ablated grooves on an FS-treated plastic surface. The laser creates grooves that lack the FS treatment, allowing the metal to selectively adhere to the plastic. (a, b) Optical images of EGaln-patterned lines. (c) Cross-section image of the patterned EGaln. (d) The resistance of the patterned EGaln vs the cross-sectional area of the pattern. The red line represents theory assuming the metal perfectly adopts the cross-sectional shape of the channels. (e, f) Three-dimensionally patterned EGaln with metallic conductivity that spans three sides of a 3D printed cube.

metal left behind residue on the uncoated portions due to pinning. In contrast, the liquid metal droplets receded completely from the coated surfaces in all cases.

Scratching the coated surface with tweezers or rubbing it by hand resulted in lost hydrophilic/metallophobic functionality. Fortunately, in the absence of harsh external abrasion, the coating remained robust while the advancing/receding experiments were repeated at least 100 times inside the 3D printed parts, which suggests the coating is useful for fluidic applications. The FS-coated substrate remained metallophobic after being stored in ambient conditions over a year. Moreover, as the coating layer is quite thin and adheres directly to the polymer surface, the coating hardly changes the optical transparency of the plastics (Figure 4g–i). In contrast, rough surfaces and coatings used previously to prevent metal adhesion typically scatter light and appear hazy (e.g., Neverwet).⁴⁹

As shown by control experiments, the metal adheres to nontreated regions, which is useful for patterning.^{47,56,57} First, we coated the exterior surface of a 3D printed part and laser-patterned recesses into the polymer surface. The laser treatment not only ablates the polymer but also removes the coating from the exposed regions. The liquid metal wets only the ablated region, which lacks the coating (Figure 5a). The smallest features created by the laser are 100 μm wide (Figure 5b). We investigated the geometry of the ablated parts at varying power and speed using the laser engraver (VLS 3.50, ULS), as shown in Figure S6. After the recesses were patterned, EGaln was placed on the surface (Figure S7a), and then the substrate was gently tapped to facilitate contact between EGaln and the inner surface (Figure S7b). Because the inertia of the liquid metal does not cause it to penetrate the

FS coating (as established by Figure 3), it only penetrated the ablated channels.

It was possible to remove the conductive pathway completely by applying strong acid or base (Figure S7c–e). Patterning and erasing EGaln was also repeatable, as the coating layer is resistive to the acid or base over the short time scales necessary to remove the oxide. We measured the electrical resistance of the patterned liquid metal and compared it to the theoretical value of the resistance with the assumption of an EGaln/air/plastic configuration, as shown in Figure 5c,d. The theoretical value of the resistance follows Pouillet's law ($R = \rho l/A$, where ρ is the resistivity, l is the length, and A is the cross-sectional area). Thus, resistance is inversely proportional to the cross-sectional area (red curve in Figure 5d). However, the cross-sectional area of the patterned metal is not the same as that of the ablated trench. If the depth of the trench is deep (i.e., 80% power and 50% speed case, see Figure S6d), there are gaps between the patterned metal and plastic so that the resistance of the patterned metal is higher than that of the theoretical value. Conversely, if the depth of the trench is too shallow (i.e., 20% power and 50% speed, see Figure S6a), the patterned liquid metal can overflow the trench, thereby making the resistance lower than that of the theoretical value. When the depth of the cross-section of the trench is smaller than 126 μm (60% power and 50% speed), the EGaln–air interface was no longer flush with the plastic surface (instead, it had a hemispherical meniscus), resulting in a smaller resistance than the theoretically calculated value.

We prepared a three-dimensional circuit using the selectively patterned liquid metal, as shown in Figure 5e,f. The part consists of a printed cube (30 mm \times 30 mm \times 30 mm) coated with FS and subsequently ablated in a zigzag pattern by a laser

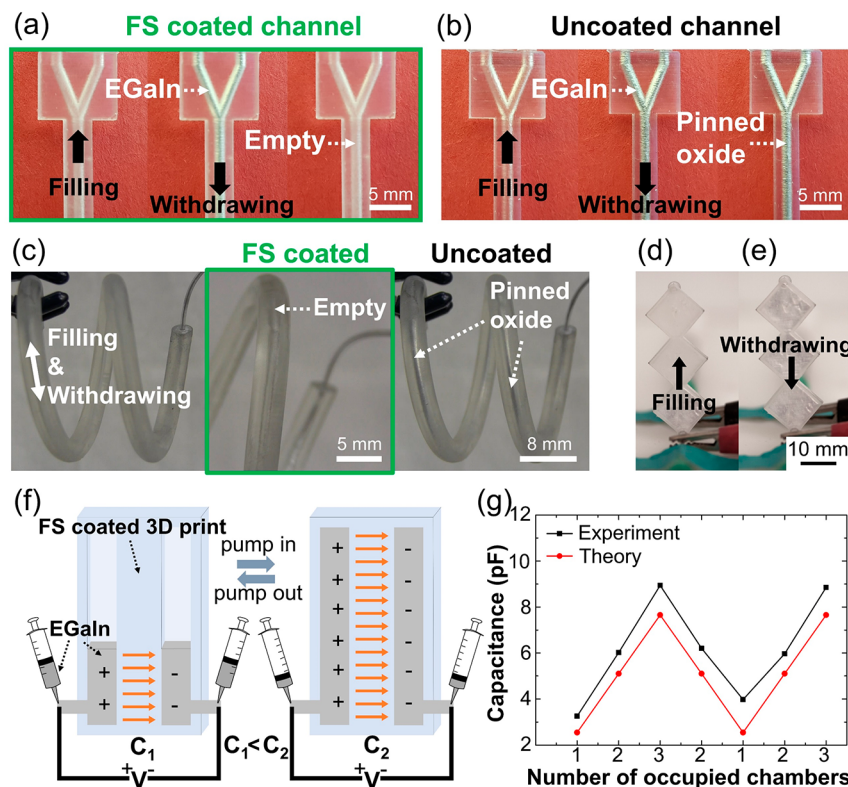


Figure 6. Solution-based coating can be applied inside of 3D printed structures to create reconfigurable circuits. (a, c) EGaln can be pumped in and out of coated 3D printed channels without leaving residue or pinning. (b, c) EGaln sticks to the surface of the uncoated channel and cannot be withdrawn without leaving residue. (d, e) The variable-area parallel capacitor achieved by filling and withdrawing EGaln from the chambers. (f) Schematic of a variable-area parallel capacitor consisting of rhombus-shaped chambers that feature an inlet at the bottom for injecting liquid metal. (g) The capacitance of the variable-area parallel capacitor with a varying number of occupied chambers. Capacitance was proportional to the area of the capacitor and showed a stable repeatability owing to pinning-free behavior of EGaln.

on three faces. The three-dimensionally patterned liquid metal wiring powered a blue light-emitting diode (LED) to demonstrate electrical continuity.

One appeal of this coating is the ability to treat the channel or cavity walls of interior structures that are inaccessible to most other treatments to make surfaces rough. To demonstrate that the coating can be applied to the inner surface of the 3D printed plastic, we printed a Y-shaped channel and a coaxial (hollow) helix with a 1.5 mm diameter. The coating solution easily filled the channel and created a coating similar to the ones described on flat, exposed surfaces. As shown in Figure 6a,c, the EGaln did not adhere to the inner surface of the channel and could be pumped in/out of the channel without leaving a residue. In contrast, if the channel was not coated, the EGaln pinned within the channel (Figure 6b,c).

The coating also applies readily to thermoplastic microchannels with dimensions smaller than those from 3D printing. We prepared a metallophobic microchannel with a diameter of $\sim 300 \mu\text{m}$ by assembling two laser-ablated PMMA sheets, followed by injection of the FS solution. EGaln did not pin to the treated microchannel (Figure S8a,b). We tried to create even smaller channels using SU-8 (a negative photoresist commonly used for microfabrication) or poly(dimethylsiloxane) (PDMS), but the coating method does not work well on polymers that are heavily cross-linked or have a low glass transition temperature since the coating relies on temporal plasticization of the polymer.

To demonstrate a reconfigurable circuit, we designed a variable-area parallel capacitor as shown in Figure 6d–g. To

modulate the area of the capacitor, EGaln can be pumped in and out of the three rhombus-shaped chambers (10 mm by 10 mm) connected serially. According to Figure 6f, the capacitance of the variable-area parallel capacitor was directly proportional to the number of filled chambers as shown in Figure 6g, though the experimental results are slightly larger than the theoretical results, presumably due to the fringing fields from the edge of the capacitor.

CONCLUSION

Gallium-based liquid metals tend to pin on most solid surfaces due to a thin native oxide layer. We report a simple way to coat fumed silica on many plastics—including those commonly used in 3D printed parts—thereby rendering the surfaces of the plastics metallophobic (i.e., gallium-based liquid metals featuring surface oxides do not adhere to it). Whereas most roughened surfaces (e.g., super-hydrophobic surfaces) are hazy or opaque, the coating here is completely transparent. Whereas prior approaches work well for coating exposed, exterior surfaces, the work here is unique because of the ability to coat the interior of plastic cavities, since it is a solution-based treatment. We proved that liquid metal does not adhere to these surfaces by (1) measuring advancing/receding behavior, (2) showing that the liquid metal rolls off the coated plastics at a 15° incline, and (3) observing that liquid metal bounces off the coated surface when dropped from 70 cm. Advancing and receding the metal more than 100 times across the surface without pinning suggests the adhesion of the fumed silica and the substrate is sufficiently robust for fluidic applications. To

demonstrate a new application, we pneumatically actuated liquid metal in a coated 3D printed chamber without leaving behind a residue to create a variable-area capacitor. These shape-reconfigurable circuits within 3D printed parts are a promising alternative for 4D printing concepts that utilize electronics and thermal components. The metal can move in sync with shape changes of the 4D printed parts, or the metal can be pumped in or out of capillaries built into 3D printed parts to create time-varying metallic components. In addition to coating the interior of 3D printed parts, it is possible to selectively remove the coating from the exterior using laser ablation to achieve selective wetting and thereby pattern liquid metal on the exterior of 3D printed plastics.

■ EXPERIMENTAL SECTION

Materials. Eutectic gallium–indium alloy (EGaIn) was purchased from Indium Corporation. Fumed silica (Aerosil 150, Evonik Industries) was purchased from Evonik. IPA was purchased from VWR. Toluene, tetrahydrofuran (THF), and chloroform were purchased from Sigma-Aldrich. Unless otherwise specified, the chemicals used in the current work were used without further purification.

Preparation of Fumed Silica-3D Printed Plastic. *a. Preparation of the 3D Printed Plastics.* The clear resin was printed using a commercial 3D printer (Form2, Formlabs) with a layer thickness of 25 μm . A 405 nm UV beam selectively cured the resin for each layer. Clear resin (RS-F2-GPCL-04) enabled visual inspection of the EGaIn inside the channel. After the printing, the part was immersed in an IPA bath for 30 min to remove residual resin, uncured monomer, and initiators. Two other commercial printers were also utilized to show the diverse range of the process; B9 Creator (B9 Creations, DLP type) with resin (B9R-1-Red) and Lulzbot Taz 6 (Aleph Objects, Inc., FDM type) with poly(lactic acid) filament.

b. Coating Process of the Fumed Silica on the Print. A fumed silica (1% w/v) was freshly dispersed in the appropriate organic solvent determined empirically. As the fumed silica is hydrophilic, polar organic solvents were used. For the clear resin, chloroform was used, yet THF was also a good solvent for the fumed silica. For the ABS-based polymer, a chloroform/IPA (50% v/v) mixture was used. For the PLA-based polymer, a chloroform/toluene (50% v/v) mixture was used. After the fumed silica and the solvent were mixed, bath sonication was applied for 30 min to improve the dispersity of the fumed silica. The plastics were immersed in each solution for 2 min, and then they were rinsed with IPA and water and dried completely using compressed air. Without the rinsing steps, the fume silica formed large agglomerates, resulting in a deposition of excess fumed silica.

Characterization of the Fumed Silica. Transmission electron microscopy (TEM) was employed to visualize the fumed silica. The fumed silica solution in chloroform (0.01% w/v) was prepared, and then a bath sonication was applied for 30 min. The solutions were drop-casted on a holey carbon-coated TEM grid for imaging. The TEM grids were stored in a desiccator for 1 d to eliminate the solvent. The images were collected using a high-resolution TEM (F20, FEI) at an acceleration voltage of 200 kV. The TEM images were analyzed by using ImageJ to calculate the distribution of the size of individual silica particles.

Characterization of the Fumed Silica-Coated Surface. A plastic substrate with dimensions of 8 mm \times 8 mm \times 2 mm (width \times length \times thickness) was printed, and then the plastic was coated with the fumed silica as described in the previous paragraph. Scanning electron microscopy (SEM) was utilized to image the fumed silica-coated surfaces. The morphology of the samples was observed by SEM (SUPRA 55VP, Carl Zeiss). Atomic force microscopy (AFM) measurements were performed with Veeco Dimension 3000 (Veeco Digital Instruments) under ambient conditions. Tapping mode was used, and the scanning area was 10 μm \times 10 μm . Fourier transform infrared (FT-IR) spectra in the 600–4000 cm^{-1} frequency range and

a step of 4 cm^{-1} were recorded using a Nicolet iS 9 FT-IR spectrometer (Thermo Scientific) operating in the attenuated total reflection (ATR) mode.

EGaIn Droplet Bouncing Observation using a High-Speed Camera. An EGaIn droplet ($\sim 5 \mu\text{L}$) was dispensed by using a 30-gauge needle and dropped above the fumed silica-coated/uncoated plastics. A high-speed camera (Phantom v4.2, Vision Research) was used to capture a video of the impact at a rate of 2200 frames per second.

Selective Patterning of the EGaIn and Electrical Measurement. After the plastics were printed, they were coated with the fumed silica as described in the previous paragraph. Then, various patterns were ablated with a commercial laser writing system (VLS 3.50, Universal Laser Systems) with a 40 W CO_2 laser operating at 10.6 μm . The geometry of the trenches depends on the speed and the power of the head. Typically, 20% power and 30% speed was utilized for the channel of 150 μm width. After EGaIn covered the whole area of the substrate, it was tapped several times on a rigid table to promote EGaIn to enter the trenches. Then, EGaIn was suctioned into a syringe to leave EGaIn only on the ablated area. The resistance of the patterned EGaIn was measured by a multimeter (2400, Keithley). The capacitance of the variable-area parallel capacitor was measured by a capacitance meter (U1733C, Agilent)

■ ASSOCIATED CONTENT

Supporting Information

The Supporting Information is available free of charge at <https://pubs.acs.org/doi/10.1021/acsami.0c17283>.

Supporting video (MP4)

Supporting video (MP4)

Supporting video (MP4)

Supporting video (MP4)

Swelling behavior of the polymer, AFM scan curve, the high-speed camera setup for EGaIn drop test, cross-sectional images of the laser-ablated plastic, solvent compositions for the various plastics, recycling of the patterning process, FS-coated microfluidic channel (PDF)

■ AUTHOR INFORMATION

Corresponding Author

Michael D. Dickey – Department of Chemical and Biomolecular Engineering, North Carolina State University, Raleigh 27695, North Carolina, United States; orcid.org/0000-0003-1251-1871; Email: mddickey@ncsu.edu

Authors

Jinwoo Ma – Department of Chemical and Biomolecular Engineering, North Carolina State University, Raleigh 27695, North Carolina, United States; orcid.org/0000-0001-5140-2972

Vivek T. Bharambe – Department of Electrical and Computer Engineering, North Carolina State University, Raleigh 27695, North Carolina, United States

Karl A. Persson – Department of Chemical and Biomolecular Engineering, North Carolina State University, Raleigh 27695, North Carolina, United States

Adam L. Bachmann – Department of Chemical and Biomolecular Engineering, North Carolina State University, Raleigh 27695, North Carolina, United States

Ishan D. Joshipura – Department of Chemical and Biomolecular Engineering, North Carolina State University, Raleigh 27695, North Carolina, United States

Jongbeom Kim – Department of Material Science and Engineering, Seoul National University, Seoul 151-742, South Korea

Kyu Hwan Oh – Department of Material Science and Engineering, Seoul National University, Seoul 151-742, South Korea

Jason F. Patrick – Department of Civil, Construction, and Environmental Engineering, North Carolina State University, Raleigh 27695, North Carolina, United States

Jacob J. Adams – Department of Electrical and Computer Engineering, North Carolina State University, Raleigh 27695, North Carolina, United States

Complete contact information is available at:
<https://pubs.acs.org/10.1021/acsami.0c17283>

Author Contributions

M.D.D. and J.J.A. conceived the project and directed it. J.M. performed a majority of the sample preparation and characterized the metallophobicity of the surface. V.T.B. characterized the electrical properties of the pattern. K.A.P. and I.D.J. performed the advancing and receding of the liquid metal. A.L.B. performed AFM measurement. J.K. performed SEM and TEM under the guidance of K.H.O.; J.M., J.F.P., and M.D.D. wrote the manuscript with inputs from all authors.

Notes

The authors declare no competing financial interest.

ACKNOWLEDGMENTS

The authors acknowledge support from the National Science Foundation and the U.S. Army Research Office under Grant No. W911NF-17-1-0216. This work was supported by Korea Evaluation Institute of Industrial Technology and the Ministry of Trade, Industry & Energy of the Republic of Korea (No. 1415168877).

REFERENCES

- (1) Dickey, M. D. Stretchable and Soft Electronics using Liquid Metals. *Adv. Mater.* **2017**, *29* (27), 1606425.
- (2) Song, M.; Kartawira, K.; Hillaire, K. D.; Li, C.; Eaker, C. B.; Kiani, A.; Daniels, K. E.; Dickey, M. D. Overcoming Rayleigh–Plateau instabilities: Stabilizing and destabilizing liquid-metal streams via electrochemical oxidation. *Proc. Natl. Acad. Sci. U. S. A.* **2020**, *117* (32), 19026–19032.
- (3) Han, J.; Tang, J.; Idrus-Saidi, S. A.; Christoe, M. J.; O'Mullane, A. P.; Kalantar-Zadeh, K. Exploring Electrochemical Extrusion of Wires from Liquid Metals. *ACS Appl. Mater. Interfaces* **2020**, *12*, 31010–31020.
- (4) Thrasher, C. J.; Farrell, Z. J.; Morris, N. J.; Willey, C. L.; Tabor, C. E. Mechanoresponsive Polymerized Liquid Metal Networks. *Adv. Mater.* **2019**, *31* (40), 1903864.
- (5) Jin, Y.; Lin, Y.; Kiani, A.; Joshipura, I. D.; Ge, M.; Dickey, M. D. Materials tactile logic via innervated soft thermochromic elastomers. *Nat. Commun.* **2019**, *10* (1), 4187.
- (6) Kim, M.-g.; Brown, D. K.; Brand, O. Nanofabrication for All-Soft and High-Density Electronic Devices based on Liquid Metal. *Nat. Commun.* **2020**, *11* (1), 1002.
- (7) Liu, S.; Yuen, M. C.; White, E. L.; Boley, J. W.; Deng, B.; Cheng, G. J.; Kramer-Bottiglio, R. Laser Sintering of Liquid Metal Nanoparticles for Scalable Manufacturing of Soft and Flexible Electronics. *ACS Appl. Mater. Interfaces* **2018**, *10* (33), 28232–28241.
- (8) Krisnadi, F.; Nguyen, L. L.; Ankit, Ma, J.; Kulkarni, M. R.; Mathews, N.; Dickey, M. D. Directed Assembly of Liquid Metal–Elastomer Conductors for Stretchable and Self-Healing Electronics. *Adv. Mater.* **2020**, *32*, 2001642.

(9) Kazem, N.; Hellebrekers, T.; Majidi, C. Soft Multifunctional Composites and Emulsions with Liquid Metals. *Adv. Mater.* **2017**, *29* (27), 1605985.

(10) Markvicka, E. J.; Bartlett, M. D.; Huang, X.; Majidi, C. An Autonomously Electrically Self-Healing Liquid Metal–Elastomer Composite for Robust Soft-Matter Robotics and Electronics. *Nat. Mater.* **2018**, *17* (7), 618–624.

(11) Pan, C.; Markvicka, E. J.; Malakooti, M. H.; Yan, J.; Hu, L.; Matyjaszewski, K.; Majidi, C. A Liquid-Metal–Elastomer Nanocomposite for Stretchable Dielectric Materials. *Adv. Mater.* **2019**, *31* (23), 1900663.

(12) Ma, J.; Lin, Y.; Kim, Y.-W.; Ko, Y.; Kim, J.; Oh, K. H.; Sun, J.-Y.; Gorman, C. B.; Voinov, M. A.; Smirnov, A. I.; Genzer, J.; Dickey, M. D. Liquid Metal Nanoparticles as Initiators for Radical Polymerization of Vinyl Monomers. *ACS Macro Lett.* **2019**, *8* (11), 1522–1527.

(13) Yun, G.; Tang, S.-Y.; Sun, S.; Yuan, D.; Zhao, Q.; Deng, L.; Yan, S.; Du, H.; Dickey, M. D.; Li, W. Liquid Metal-Filled Magnetorheological Elastomer with Positive Piezoconductivity. *Nat. Commun.* **2019**, *10* (1), 1300.

(14) Abbasi, R.; Mayyas, M.; Ghasemian, M. B.; Centurion, F.; Yang, J.; Saborio, M.; Allieux, F.-M.; Han, J.; Tang, J.; Christoe, M. J.; Mohibul Kabir, K. M.; Kalantar-Zadeh, K.; Rahim, M. A. Photolithography-enabled direct patterning of liquid metals. *J. Mater. Chem. C* **2020**, *8*, 7805.

(15) Liang, S.-T.; Wang, H.-Z.; Liu, J. Progress, Mechanisms and Applications of Liquid-Metal Catalyst Systems. *Chem. - Eur. J.* **2018**, *24* (67), 17616–17626.

(16) Esrafilzadeh, D.; Zavabeti, A.; Jalili, R.; Atkin, P.; Choi, J.; Carey, B. J.; Brkljača, R.; O'Mullane, A. P.; Dickey, M. D.; Officer, D. L.; MacFarlane, D. R.; Daeneke, T.; Kalantar-Zadeh, K. Room Temperature CO₂ Reduction to Solid Carbon Species on Liquid Metals Featuring Atomically Thin Ceria Interfaces. *Nat. Commun.* **2019**, *10* (1), 865.

(17) Daeneke, T.; Khoshmanesh, K.; Mahmood, N.; de Castro, I. A.; Esrafilzadeh, D.; Barrow, S. J.; Dickey, M. D.; Kalantar-zadeh, K. Liquid Metals: Fundamentals and Applications in Chemistry. *Chem. Soc. Rev.* **2018**, *47* (11), 4073–4111.

(18) So, J.-H.; Thelen, J.; Qusba, A.; Hayes, G. J.; Lazzi, G.; Dickey, M. D. Reversibly Deformable and Mechanically Tunable Fluidic Antennas. *Adv. Funct. Mater.* **2009**, *19* (22), 3632–3637.

(19) Hirsch, A.; Michaud, H. O.; Gerratt, A. P.; de Mulatier, S.; Lacour, S. P. Intrinsically Stretchable Biphasic (Solid–Liquid) Thin Metal Films. *Adv. Mater.* **2016**, *28* (22), 4507–4512.

(20) Li, G.; Wu, X.; Lee, D.-W. Selectively Plated Stretchable Liquid Metal Wires for Transparent Electronics. *Sens. Actuators, B* **2015**, *221*, 1114–1119.

(21) Pan, C.; Kumar, K.; Li, J.; Markvicka, E. J.; Herman, P. R.; Majidi, C. Visually Imperceptible Liquid-Metal Circuits for Transparent, Stretchable Electronics with Direct Laser Writing. *Adv. Mater.* **2018**, *30* (12), 1706937.

(22) Deng, S.; Wu, J.; Dickey, M. D.; Zhao, Q.; Xie, T. Rapid Open-Air Digital Light 3D Printing of Thermoplastic Polymer. *Adv. Mater.* **2019**, *31* (39), 1903970.

(23) Shen, J.; Parekh, D. P.; Dickey, M. D.; Ricketts, D. S. In *3D Printed Coaxial Transmission Line Using Low Loss Dielectric and Liquid Metal Conductor*, 2018 IEEE/MTT-S International Microwave Symposium–IMS, June 10–15, 2018; IEEE, 2018; pp 59–62.

(24) Barambe, V.; Parekh, D. P.; Ladd, C.; Moussa, K.; Dickey, M. D.; Adams, J. J. Liquid-Metal-Filled 3-D Antenna Array Structure With an Integrated Feeding Network. *IEEE Antennas and Wireless Propagation Letters* **2018**, *17* (5), 739–742.

(25) Yu, Y.-Z.; Lu, J.-R.; Liu, J. 3D Printing for Functional Electronics by Injection and Package of Liquid Metals into Channels of Mechanical Structures. *Mater. Des.* **2017**, *122*, 80–89.

(26) Cosker, M.; Lizzi, L.; Ferrero, F.; Staraj, R.; Ribero, J. Realization of 3-D Flexible Antennas Using Liquid Metal and Additive Printing Technologies. *IEEE Antennas and Wireless Propagation Letters* **2017**, *16*, 971–974.

- (27) Barambe, V.; Parekh, D. P.; Ladd, C.; Moussa, K.; Dickey, M. D.; Adams, J. J. Vacuum-filling of Liquid Metals for 3D Printed RF Antennas. *Additive Manufacturing* **2017**, *18*, 221–227.
- (28) Shen, J.; Ricketts, D. S. Additive Manufacturing of Complex Millimeter-Wave Waveguides Structures Using Digital Light Processing. *IEEE Trans. Microwave Theory Tech.* **2019**, *67* (3), 883–895.
- (29) Alkaraki, S.; Andy, A. S.; Gao, Y.; Tong, K.; Ying, Z.; Donnan, R.; Parini, C. Compact and Low-Cost 3-D Printed Antennas Metalized Using Spray-Coating Technology for 5G mm-Wave Communication Systems. *IEEE Antennas and Wireless Propagation Letters* **2018**, *17* (11), 2051–2055.
- (30) Salas-Barenys, A.; Vidal, N.; Siero, J.; López-Villegas, J. M.; Medina-Rodriguez, B.; Ramos, F. M. In *Full-3D Printed Electronics Process using Stereolithography and Electroless Plating*, 32nd Conference on Design of Circuits and Integrated Systems (DCIS), November 22–24, 2017; IEEE, 2017; pp 1–4.
- (31) Massoni, E.; Guareschi, M.; Bozzi, M.; Perregrini, L.; Tamburini, U. A.; Alaimo, G.; Marconi, S.; Auricchio, F.; Tomassoni, C. In *3D Printing and Metalization Methodology for High Dielectric Resonator Waveguide Microwave Filters*, 2017 IEEE MTT-S International Microwave Workshop Series on Advanced Materials and Processes for RF and THz Applications (IMWS-AMP), September 20–22, 2017; IEEE, 2017; pp 1–3.
- (32) Ghazali, M. I. M.; Gutierrez, E.; Myers, J. C.; Kaur, A.; Wright, B.; Chahal, P. In *Affordable 3D Printed Microwave Antennas*, Proceedings of the 2015 IEEE 65th Electronic Components and Technology Conference (ECTC), May 26–29, 2015; IEEE, 2015; pp 240–246.
- (33) Dickey, M. D.; Chiechi, R. C.; Larsen, R. J.; Weiss, E. A.; Weitz, D. A.; Whitesides, G. M. Eutectic Gallium-Indium (EGaIn): A Liquid Metal Alloy for the Formation of Stable Structures in Microchannels at Room Temperature. *Adv. Funct. Mater.* **2008**, *18* (7), 1097–1104.
- (34) Barambe, V. T.; Ma, J.; Dickey, M. D.; Adams, J. J. Planar, Multifunctional 3D Printed Antennas Using Liquid Metal Parasitics. *IEEE Access* **2019**, *7*, 134245–134255.
- (35) Liu, T.; Sen, P.; Kim, C. Characterization of Nontoxic Liquid-Metal Alloy Galinstan for Applications in Microdevices. *J. Microelectromech. Syst.* **2012**, *21* (2), 443–450.
- (36) Huff, G. H.; Pan, H.; Hartl, D. J.; Frank, G. J.; Bradford, R. L.; Baur, J. W. A Physically Reconfigurable Structurally Embedded Vascular Antenna. *IEEE Trans. Antennas Propag.* **2017**, *65* (5), 2282–2288.
- (37) Kim, D.; Pierce, R. G.; Henderson, R.; Doo, S. J.; Yoo, K.; Lee, J.-B. Liquid metal actuation-based reversible frequency tunable monopole antenna. *Appl. Phys. Lett.* **2014**, *105* (23), 234104.
- (38) Khan, M. R.; Trlica, C.; So, J.-H.; Valeri, M.; Dickey, M. D. Influence of Water on the Interfacial Behavior of Gallium Liquid Metal Alloys. *ACS Appl. Mater. Interfaces* **2014**, *6* (24), 22467–22473.
- (39) Sivan, V.; Tang, S.-Y.; O'Mullane, A. P.; Petersen, P.; Eshtiaghi, N.; Kalantar-zadeh, K.; Mitchell, A. Liquid Metal Marbles. *Adv. Funct. Mater.* **2013**, *23* (2), 144–152.
- (40) Chen, Y.; Liu, Z.; Zhu, D.; Handschuh-Wang, S.; Liang, S.; Yang, J.; Kong, T.; Zhou, X.; Liu, Y.; Zhou, X. Liquid Metal Droplets with High Elasticity, Mobility and Mechanical Robustness. *Mater. Horiz.* **2017**, *4* (4), 591–597.
- (41) Chen, Y.; Zhou, T.; Li, Y.; Zhu, L.; Handschuh-Wang, S.; Zhu, D.; Zhou, X.; Liu, Z.; Gan, T.; Zhou, X. Robust Fabrication of Nonstick, Noncorrosive, Conductive Graphene-Coated Liquid Metal Droplets for Droplet-Based, Floating Electrodes. *Adv. Funct. Mater.* **2018**, *28* (8), 1706277.
- (42) Jeon, J.; Lee, J.; Chung, S. K.; Kim, D. Magnetic Liquid Metal Marble: Characterization of Lyophobicity and Magnetic Manipulation for Switching Applications. *J. Microelectromech. Syst.* **2016**, *25* (6), 1050–1057.
- (43) Kim, D.; Lee, D.; Choi, W.; Lee, J. A Super-Lyophobic 3-D PDMS Channel as a Novel Microfluidic Platform to Manipulate Oxidized Galinstan. *J. Microelectromech. Syst.* **2013**, *22* (6), 1267–1275.
- (44) Kramer, R. K.; Majidi, C.; Wood, R. J. Masked Deposition of Gallium-Indium Alloys for Liquid-Embedded Elastomer Conductors. *Adv. Funct. Mater.* **2013**, *23* (42), 5292–5296.
- (45) Kim, D.; Jung, D.; Yoo, J. H.; Lee, Y.; Choi, W.; Lee, G. S.; Yoo, K.; Lee, J.-B. Stretchable and Nendable Carbon Nanotube on PDMS Super-Lyophobic Sheet for Liquid Metal Manipulation. *J. Microelectromech. Syst.* **2014**, *24* (5), 055018.
- (46) Kramer, R. K.; Boley, J. W.; Stone, H. A.; Weaver, J. C.; Wood, R. J. Effect of Microtextured Surface Topography on the Wetting Behavior of Eutectic Gallium–Indium Alloys. *Langmuir* **2014**, *30* (2), 533–539.
- (47) Jiang, Y.; Su, S.; Peng, H.; Sing Kwok, H.; Zhou, X.; Chen, S. Selective Wetting/Dewetting for Controllable Patterning of Liquid Metal Electrodes for All-Printed Device Application. *J. Mater. Chem. C* **2017**, *5* (47), 12378–12383.
- (48) Kadlaskar, S. S.; Yoo, J. H.; Abhijeet; Lee, J. B.; Choi, W. Cost-Effective Surface Modification for Galinstan® Lyophobicity. *J. Colloid Interface Sci.* **2017**, *492*, 33–40.
- (49) Joshipura, I. D.; Ayers, H. R.; Castillo, G. A.; Ladd, C.; Tabor, C. E.; Adams, J. J.; Dickey, M. D. Patterning and Reversible Actuation of Liquid Gallium Alloys by Preventing Adhesion on Rough Surfaces. *ACS Appl. Mater. Interfaces* **2018**, *10* (51), 44686–44695.
- (50) Chen, Z.; Lee, J. B. Surface Modification with Gallium Coating as Nonwetting Surfaces for Gallium-Based Liquid Metal Droplet Manipulation. *ACS Appl. Mater. Interfaces* **2019**, *11* (38), 35488–35495.
- (51) Yao, Y. Y.; Ding, Y. J.; Li, H. P.; Chen, S.; Guo, R.; Liu, J. Multi-Substrate Liquid Metal Circuits Printing via Superhydrophobic Coating and Adhesive Patterning. *Adv. Eng. Mater.* **2019**, *21* (7), 1801363.
- (52) Agarwal, A.; Tomozawa, M. Correlation of Silica Glass Properties with the Infrared Spectra. *J. Non-Cryst. Solids* **1997**, *209* (1), 166–174.
- (53) Schaefer, D. W.; Hurd, A. J. Growth and Structure of Combustion Aerosols: Fumed Silica. *Aerosol Sci. Technol.* **1990**, *12* (4), 876–890.
- (54) Deng, X.; Mammen, L.; Butt, H.-J.; Vollmer, D. Candle Soot as a Template for a Transparent Robust Superamphiphobic Coating. *Science* **2012**, *335* (6064), 67–70.
- (55) Plech, A.; Klemradt, U.; Metzger, H.; Peisl, J. In situ X-ray Reflectivity Study of the Oxidation Kinetics of Liquid Gallium and the Liquid Alloy. *J. Phys.: Condens. Matter* **1998**, *10* (5), 971–982.
- (56) Yong, J.; Zhang, C.; Bai, X.; Zhang, J.; Yang, Q.; Hou, X.; Chen, F. Designing “Supermetalphobic” Surfaces that Greatly Repel Liquid Metal by Femtosecond Laser Processing: Does the Surface Chemistry or Microstructure Play a Crucial Role? *Adv. Mater. Interfaces* **2020**, *7* (6), 1901931.
- (57) Zhang, J.; Zhang, K.; Yong, J.; Yang, Q.; He, Y.; Zhang, C.; Hou, X.; Chen, F. Femtosecond Laser Preparing Patternable Liquid-Metal-Repellent Surface for Flexible Electronics. *J. Colloid Interface Sci.* **2020**, *578*, 146–154.